Dynamically generated resonances from the vector octet-baryon decuplet interaction

Sourav Sarkar[1,2], Bao-Xi Sun[1,3], E. Oset[1] and M.J. Vicente Vacas[1]

September 24, 2009

[1] Departamento de Física Teórica and IFIC, Centro Mixto Universidad de Valencia-CSIC, Institutos de Investigación de Paterna, Aptdo. 22085, 46071 Valencia, Spain
[2] Variable Energy Cyclotron Centre, 1/AF, Bidhannagar, Kolkata 700064, India
[3] Institute of Theoretical Physics, College of Applied Sciences, Beijing University of Technology, Beijing 100124, China

Abstract

We study the interaction of the octet of vector mesons with the decuplet of baryons using Lagrangians of the hidden gauge theory for vector interactions. The unitary amplitudes in coupled channels develop poles that can be associated with some known baryonic resonances, while there are predictions for new ones at the energy frontier of the experimental research. The work offers guidelines on how to search for these resonances.

1 Introduction

The combination of chiral Lagrangians with nonperturbative unitary techniques in coupled channels has been very fruitful and has provided a powerful tool to study meson meson and meson baryon interactions beyond the realm of applicability of chiral perturbation theory. It leads to accurate cross sections for meson meson and meson baryon interactions and allows one to study the analytical properties of the scattering matrix, where poles are sometimes found, which can be associated to known resonances or new ones. Examples of this are the low lying scalar states found in the case of meson meson interaction [1, 2, 3, 4], the $J^P = 1/2^-$ low lying baryon states found in the interaction of pseudoscalar mesons with baryons of the octet of the p [5, 6, 7, 8, 9, 10, 11, 12, 13, 14], and the $J^P = 3/2^-$ states obtained form the interaction of pseudoscalar mesons with the decuplet of baryons of the Δ [15, 16]. As an example of new states predicted, one has a second $\Lambda(1405)$ state [17], right now reconfirmed by all the chiral unitary calculations, and which finds experimental support from the analysis of the $K^- p \to \pi^0\pi^0\Sigma^0$ reaction [18] done in [19]. It also finds an

explanation for the new COSY data on $\Lambda(1405)$ production in pp collisions [20] as shown in [21].

The work with vector mesons was for some time limited to the study of their interaction with pseudoscalar mesons, which generates the low lying axial vector mesons [22, 23] and a second $K_1(1270)$ state [23], for which experimental evidence is found in [24].

A qualitative step in the interaction of vector mesons and generation of resonances was done in [25], where by using the Lagrangians of the hidden gauge approach to vector interactions [26, 27, 28], one scalar and a tensor meson were found from the $\rho\rho$ interactions, which could be identified with the $f_0(1370)$ and $f_2(1270)$ mesons, and for which the partial decay width into the sensitive $\gamma\gamma$ decay channel was found to agree with experiment [29]. An extension to the full interaction of the octet of vector mesons among themselves has been recently done [30], indicating that several scalar, axial vectors and tensor states reported in the PDG [31] qualify as dynamically generated states from the vector-vector interaction.

In the baryon sector the interaction of vector mesons with baryons leading to generation of resonances was first done in [32] for the case of the $\rho\Delta$ interaction, which leads to three N^* and three Δ^* states in the vicinity of 1900 MeV, which are degenerate in $J^P = 1/2^-, 3/2^-, 5/2^-$ within the approximations done, and which can be associated to existing states of the PDG.

After the successful predictions for the lowest states generated with vector mesons and baryons of the decuplet with $\rho\Delta$, the extension to the full $SU(3)$ space of vectors and members of the decuplet of baryons is most opportune and this is the purpose of the present work. We extend the work of [32], using the formalism developed there, and we find *ten* states dynamically generated, some of which can be clearly associated to known resonances, while others are less clear. The states found are also degenerate in spin, and in some cases the known states of the PDG support this finding. In other cases one or two of these spin states are found in the PDG but others are missing. The findings of the present work indicate that such spin parters should exist and this offers a new motivation for the search of new baryonic resonances with the quantum numbers predicted.

2 Formalism for VV interaction

We follow the formalism of the hidden gauge interaction for vector mesons of [26, 27, 28] (see also [45] for a practical set of Feynman rules). The Lagrangian involving the interaction of vector mesons amongst themselves is given by

$$\mathcal{L}_{III} = -\frac{1}{4}\langle V_{\mu\nu} V^{\mu\nu} \rangle \ , \tag{1}$$

where the symbol $\langle\rangle$ stands for the trace in the $SU(3)$ space and $V_{\mu\nu}$ is given by

$$V_{\mu\nu} = \partial_\mu V_\nu - \partial_\nu V_\mu - ig[V_\mu, V_\nu] \ , \tag{2}$$

where g is given by

$$g = \frac{M_V}{2f} \ , \tag{3}$$

with $f = 93\, MeV$ the pion decay constant. V_μ corresponds to the $SU(3)$ matrix of the vectors of the octet of the ρ with the mixing of ϕ and ω accounted for and is given by

$$V_\mu = \begin{pmatrix} \frac{\rho^0}{\sqrt{2}} + \frac{\omega}{\sqrt{2}} & \rho^+ & K^{*+} \\ \rho^- & -\frac{\rho^0}{\sqrt{2}} + \frac{\omega}{\sqrt{2}} & K^{*0} \\ K^{*-} & \bar{K}^{*0} & \phi \end{pmatrix}_\mu \ . \tag{4}$$

The interaction of $\mathcal{L}_{III}$ gives rise to a three vector vertex form

$$\mathcal{L}_{III}^{(3V)} = ig\langle (\partial_\mu V_\nu - \partial_\nu V_\mu) V^\mu V^\nu \rangle \ , \tag{5}$$

which can be conveniently rewritten using the property of the trace as

$$\mathcal{L}_{III}^{(3V)} = ig\langle [V^\mu (\partial_\nu V_\mu) - (\partial_\nu V_\mu) V^\mu] V^\nu \rangle \ . \tag{6}$$

With the three vector coupling we can construct the Feynman diagram which is responsible for the vector baryon decuplet interaction through the exchange of a vector between two vectors and the baryon, see fig. 1(b), in analogy with the interaction of a pseudoscalar meson with the baryon decuplet depicted in fig. 1(a). This mechanism of interaction of pseudoscalars with baryons, leads to the well known Weinberg-Tomozawa term, upon neglecting q^2/M_V^2 in the propagator of the exchanged vector, where q is the momentum transfer. The local chiral Lagrangian for vector baryon decuplet interaction can thus be obtained from this formalism upon neglecting the momentum transfer compared to the mass of the vector, a good approximation for the purpose of studying the interaction relatively close to threshold where bound states or resonances are searched for. Consistent with this implicit approximation of the chiral Lagrangians, we neglect the three-momentum of the vectors compared to their mass. In this approximation the polarization vectors of the vector mesons have only spatial components. This simplifies considerably the formalism. Indeed, let us look at eq. (6) where we see that the field V^ν cannot correspond to an external vector meson. Indeed, if this were the case, the ν index should be spatial and then the partial derivative ∂_ν would lead to a three momentum of the vector mesons which are neglected in the approach. Then V^ν corresponds to the exchanged vector. In this case one finds an analogy to the coupling of vectors to pseudoscalars given in the same theory by

$$\mathcal{L}_{VPP} = -ig\langle [P(\partial_\nu P) - (\partial_\nu P) P] V^\nu \rangle, \tag{7}$$

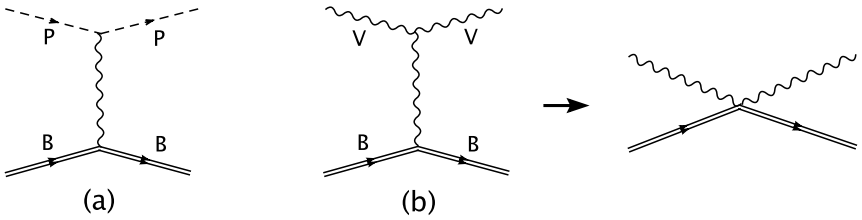

Figure 1: Diagrams contributing to the pseudoscalar-baryon (a) or vector- baryon (b) interaction via the exchange of a vector meson leading to the effective vector-baryon contact interaction which is used in the Bethe-Salpeter equation

where P is the $SU(3)$ matrix of the pseudoscalar fields. The only difference is the polarization vector of the two external fields and a sign, which recalling that we only have spatial components for the external vectors, results in the factor $\vec{\epsilon}\cdot\vec{\epsilon'}$ additional to the contribution from the PPV Lagrangian of eq. (7), from the upper vertex of fig. 1 (a).

Consequently, in order to obtain the tree level amplitudes corresponding to the diagram of fig. 1(b), all one has to do is to take the corresponding amplitudes of pseudoscalar meson-baryon decuplet interaction, substituting the $SU(3)$ pseudoscalar matrix by the corresponding one of the vector mesons. That is, $\pi^+\Delta^+ \to \pi^+\Delta^+$ is substituted by $\rho^+\Delta^+ \to \rho^+\Delta^+$ and so on.

A small amendment is in order, which is due to the mixing of ω_8 and the singlet of $SU(3)$, ω_1, to give the physical states of ω and ϕ

$$\begin{aligned}\omega &= \frac{2}{\sqrt{6}}\omega_1 + \frac{1}{\sqrt{3}}\omega_8 \\ \phi &= \frac{1}{\sqrt{3}}\omega_1 - \frac{2}{\sqrt{6}}\omega_8\end{aligned} \tag{8}$$

Given the structure of eq. (8), the singlet state which is accounted for by the V matrix, $diag(\omega_1,\omega_1,\omega_1)/\sqrt{3}$, does not provide any contribution to eq. (6), in which case, one simply has to take the matrix elements known for the PB interaction and wherever P is the η_8 multiply the amplitude by the factor $1/\sqrt{3}$ to get the corresponding ω contribution and by $-\sqrt{2/3}$ to get the corresponding ϕ contribution.

We take the matrix elements for the amplitudes from [16]. There the same approximations that we make for the vector mesons, neglecting the the three-momentum versus their mass, were also done for the baryons and then all the amplitudes have the form

$$V_{ij} = -C_{ij}\,\frac{1}{4f^2}\,(k^0 + k'^0)\;\vec{\epsilon}\cdot\vec{\epsilon'}, \tag{9}$$

where k^0, k'^0 are the energies of the incoming and outgoing vector meson respectively. The amplitudes are thus exactly the ones for $PB \to PB$ apart for the factor $\vec{\epsilon}\cdot\vec{\epsilon'}$.

The C_{ij} coefficients of eq. (9) can be obtained directly from [16] with the simple rules given above for the ω and the ϕ, and substituting π by ρ and K by K^* in the matrix elements. The coefficients are obtained both in the physical basis of states and in the isospin basis. Here we will directly study the interaction in isospin basis and we collect the tables of the C_{ij} coefficients in the Appendix for different states of isospin, I, and strangeness, S.

Inspection of the tables immediately show the cases where we find attractive interaction and we can expect bound states or resonances, and where there is repulsion no states should be expected. We find attraction in the channels $S, I = 0, 1/2;\ 0, 3/2;\ -1, 0;\ -1, 1;\ -2, 1/2$ and maybe $-3, 0$, where the diagonal terms are zero but one can get bound states through the interplay of the non diagonal terms of the coupled channels. On the other hand in the $0, 5/2;\ -1, 2;\ -2, 3/2;\ -3, 1$ and $-4, 1/2$ one finds repulsion and one should not expect bound states or resonances there. Interestingly, these are all exotic channels and we find that even if these exotic quantum numbers can be reached within the approach, for dynamical reasons, no bound states are found in either of the possible exotic channels.

As one can see, we have only considered t-channel mechanisms with the exchange of vector mesons. The strength of these terms is very large, since it is roughly proportional to the sum of two vector masses, by comparison to the interaction of pseudoscalar mesons with baryons, where the interaction is proportional to the sum of two pseudoscalar masses. One may wonder what happens with other mechanisms of u-channel type. The u-channel mechanism with the building blocks that we are using is depicted in fig. $2(a)$. Similarly we could also consider the s-channel depicted in Fig. $2(b)$. In both cases, one finds terms

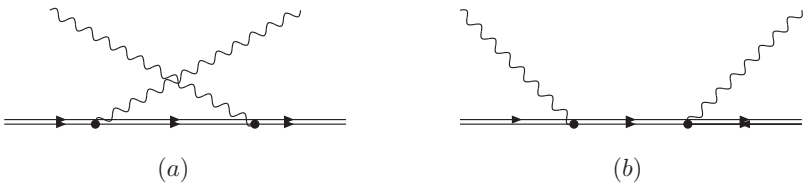

Figure 2: (a) u-channel mechanism. (b) s-channel mechanism.

of order q/M_V contributing mostly to p-waves. Since we only consider s-wave interaction and furthermore we neglect terms of q/M_V in our approach, all these terms are omitted for consistency of the whole approach. The part coming from the negative energy components of the baryon propagators in fig. $2(b)$ contributes to the s-wave, but should also be neglected for consistency with the nonrelativistic approach followed in the interaction vertices. This contribution, evaluated in [44] (see appendix of that paper), is anyway small compared to the leading terms that we have here. In the s-wave mechanism one can think of the possibility of having negative parity resonances in the intermediate state to which $\rho\Delta$ couple strongly, but these are the resonances that we are generating dynamically and, thus, those terms should be omitted to avoid double counting. We will come back to these terms in subsection 2.2.

The next step to construct the scattering matrix is done by solving the coupled channels Bethe Salpeter equation in the on shell factorization approach of [8, 9]

$$T = [1 - V\,G]^{-1}\,V \tag{10}$$

with G the loop function of a vector meson and a baryon which we calculate in dimensional regularization using the formula of [9], with μ a regularization scale of 700 MeV, and natural values of the subtraction constants $a_l(\mu)$ around -2, as determined in [9].

The on shell factorization has its root on the use of unitarity and dispersion relations. It is an exact result if one omits the contribution of the left hand cut, which is small for these processes, and in any case smoothly energy dependent in the region of interest to us, such that its contribution can be easily accommodated in terms of a subtraction constant in the dispersion integral [9] (details can be seen in this reference and for a pedagogical overview in [46], section 3). We will come back to this point in subsection 2.2.

The iteration of diagrams implicit in the Bethe Salpeter equation in the case of the vector mesons has a subtlety with respect to the case of the pseudoscalars. The $\vec{\epsilon}\cdot\vec{\epsilon}'$ term of the interaction forces the intermediate vector mesons in the loops to propagate with the spatial components in the loops. We need to sum over the polarizations of the internal vector mesons which, because they are tied to the external ones through the $\vec{\epsilon}\cdot\vec{\epsilon}'$ factor, provides

$$\sum_{pol} \epsilon_i \epsilon_j = \delta_{ij} + \frac{q_i q_j}{M_V^2} \tag{11}$$

As shown in [23], the on shell factorization leads to a correction coefficient in the G function of $\vec{q}^{\,2}/3M_V^2$ versus unity, which is negligibly small, and is also neglected here for consistency with the approximations done. In this case the factor $\vec{\epsilon}\cdot\vec{\epsilon}'$ appearing in the potential V, factorizes also in the T matrix for the external vector mesons.

Since the spin dependence only comes from the $\vec{\epsilon}\cdot\vec{\epsilon}'$ factor and there is no dependence on the spin of the baryons, the interaction for vector-baryon states with $1/2^-$, $3/2^-$ and $5/2^-$ is the same and thus we get three degenerate states for each of the resonances found. The spin degeneracy also appears in some quark models [47].

Finally, as done in [32], we take into account the convolution of the G function with the mass distributions of the ρ, K^*, Δ, $\Sigma(1385)$ and $\Xi(1530)$ states, in order to account for their sizable width.

2.1 Long range forces with intermediate vector nonet and baryon octet

In Ref. [32], in the study of the $\rho\Delta$ interaction, we evaluated explicitly the contribution of the box diagram with an intermediate $\omega\Delta$ state, with the transition $\rho\Delta \to \omega\Delta$ mediated by a pion exchange. This term turned out to be small compared with the contribution from ρ exchange. The same long range force can also produce ωN intermediate states, and in its extension to $SU(3)$, states of a nonet vector meson and an octet baryon. We

evaluate explicitly here the case of $\rho\Delta \to \omega N$, which involves the pion exchange. We will find a very small contribution, and in other cases where we exchange heavier pseudoscalar mesons one, thus, expects an even smaller contribution. The diagram that we evaluate is shown in fig. 3.

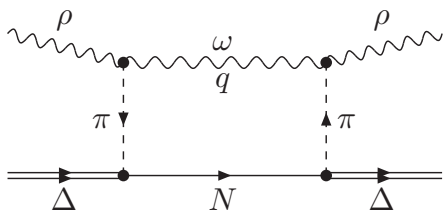

Figure 3: Term with intermediate ωN in the $\rho\Delta \to \rho\Delta$ interaction, involving the anomalous $\rho\omega\pi$ coupling and pion exchange.

We rely upon the evaluation of Ref. [32] and note here the differences. The anomalous $\rho\omega\pi$ term is the same in both cases. The only difference is the $\pi N\Delta$ vertex here versus the $\pi\Delta\Delta$ used in Ref. [32]. The $\pi N\Delta$ vertex is given by

$$-it_{\pi N\Delta} \;=\; \frac{f_{\pi N\Delta}}{m_\pi}\; \vec{S}\cdot\vec{q}\,\vec{T}\cdot\vec{\phi}, \tag{12}$$

where $\vec{S}$ and $\vec{T}$ are the spin and isospin transition operators from 3/2 to 1/2, normalized such that

$$\langle 3/2, M|S^\dagger_\nu|1/2, m\rangle \;=\; C(1/2, 1, 3/2; m, \nu, M), \tag{13}$$

and the same for $T^\dagger_\nu$, with $S^\dagger_\nu$ written in spherical basis and $C(1/2, 1, 3/2; m, \nu, M)$ the ordinary Clebsch-Gordan coefficients.

We find easily that

$$\langle \Delta\rho, I = 1/2|\vec{T}^\dagger\cdot\vec{\phi}\;\vec{T}\cdot\vec{\phi}|\Delta\rho, I = 1/2\rangle \;=\; 2. \tag{14}$$

On the other hand, for the spin part, instead of $\vec{S}^2 = 3/2\cdot 5/2$ in Ref. [32], we find now $\vec{S}^\dagger\cdot\vec{S} = 1$. Thus, we replace

$$\frac{15}{4}\times\frac{15}{4}f^2_\Delta \to 2\times 1 f^2_{\pi N\Delta}$$

with the value $f_{\pi N\Delta} = 2.23$ and $f_\Delta = 0.802$. These two coefficients are nearly equal. This is not the only change. In eq. (37) of Ref. [32], one must in addition change $E_\Delta \to E_N = \sqrt{\vec{q}^2 + M^2_N}$, wherever it appears, caring to put the $i\epsilon$ in the $(P^0 - k^0 - \omega_\pi - E_N + i\epsilon)^{-2}$ term.

The numerical results can be seen in fig. 4. We can see that compared to the term from the hidden gauge Lagrangian for $I = 1/2$ (eq. (9) and Table 2), which is shown in fig. 4, the real part of the new term is very small around 1850 MeV where the $I = 1/2$ appears, and we neglect it in the calculations. The imaginary part is also small, but it would add to the width of the $I = 1/2$ states.

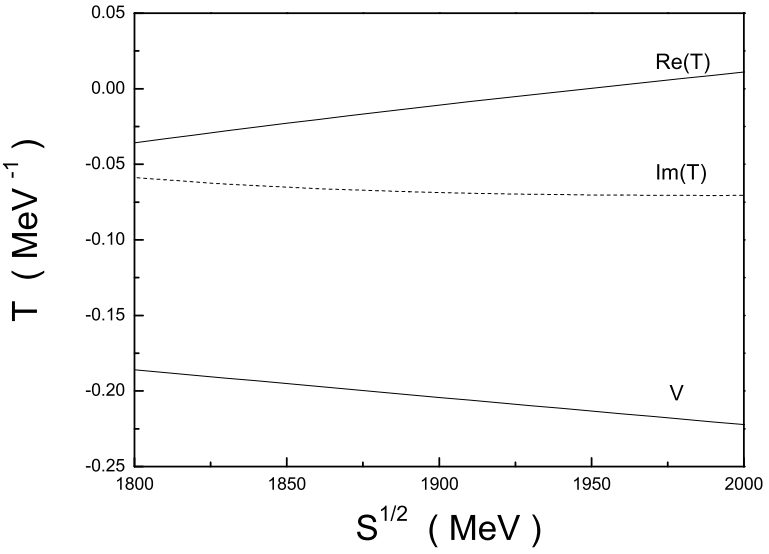

Figure 4: The real and imaginary parts of the anomalous $T_{\rho\Delta\to\rho\Delta}$ with a intermediate ωN state compared to V for $I = 1/2$ as a function of $\sqrt{s}$ for $q_{max} = 770MeV$.

2.2 Considerations on u-channel and t-channel exchanges and the on-shell factorization

The procedure followed here relies upon the on shell factorization of the amplitudes for a given energy, assuming implicitly that they come from a contact Lagrangian, and a coupled channel approach that implements unitarity in coupled channels. The method uses coupled Bethe Salpeter equations, which in this situation can be converted into algebraic equations. One way to deduce these equations is to assume the N/D method implementing dispersion relations and neglecting the contribution of the left hand cut [33, 9]. This is justified at medium energies in the interaction of light particles with heavy ones, implicitly assuming that the mass of the light particles is small compared to the mass of a hypothetical particle that is exchanged in the t-channel to provide the interaction. This is well suited for the scattering of pseudoscalar mesons off baryons [9]. The fact that we have here the scattering of vector mesons off baryons and that the interaction is driven by the exchange of vector mesons indicates that we are not in the ideal conditions like the scattering of pseudoscalar mesons and we have to find a justification for the procedure followed. To better understand the problem let us go into it in more detail.

The leading term of the potential in our case comes from the mechanism of fig. 1 where we have the explicit exchange of a vector meson. Certainly, in the approximation where q^2 has been neglected in comparison with M_V^2, with q the momentum transfer between the incoming and scattered vectors, no singularities appear in the potential. However,

removing this approximation, for certain energies below threshold and extrapolating q^2 assuming $p^2 = m^2$ for the external particles, one can have $q^2 = M_V^2$ and the propagator develops a singularity, giving rise to the branch point of the left hand cut associated with the t-channel exchange. Similarly, if one takes the diagram of fig. 2(a), and assuming again $p^2 = m^2$ for the external legs, the intermediate baryon can be placed on shell for a certain energy below threshold. The hope is that in any case these left hand cuts are far away from the energy region of interest and they lead to a weakly energy dependent contribution which can be accommodated by a subtraction constant in the dispersion relation, the idea behind [33, 9]. This, however, is not the case here.

We begin with the t-exchange mechanism of fig. 1. Let us take the case of $\rho\Delta \to \rho\Delta$ (we shall discuss other channels later on). In this case, calling k, k' the momenta of the incoming, outgoing vectors and $q = k - k'$, we see that q^0 is zero, because it is an elastic channel. On the other hand, we have with the on-shell prescription of taking $p^2 = m^2$ for the external particles,

$$|\vec{k}|^2 = \frac{[s - (m_\rho + M_\Delta)^2][s - (m_\rho - M_\Delta)^2]}{4s} \tag{15}$$

and the intermediate rho meson propagator develops a pole at the highest energy when $\vec{k}$ and $\vec{k}'$ have opposite sign and then

$$-4|\vec{k}|^2 - m_\rho^2 = 0 \tag{16}$$

where $|\vec{k}|^2$ will be negative and k purely imaginary, which leads to

$$s = \frac{1}{2}(2M_\Delta^2 + m_\rho^2 + \sqrt{12M_\Delta^2 m_\rho^2 - 3m_\rho^4}\ ) \ . \tag{17}$$

This gives us a branch point at $\sqrt{s} = 1837$ MeV. We could consider this to be far away from the region of interest, except that the lowest energy of the states that we get from this interaction has an energy around 1850 MeV.

Let us go deeper into the issue by really taking the on-shell ($p^2 = m^2$) extrapolation below threshold and then projecting the ρ-exchange potential over s-wave. This is done by means of

$$\begin{aligned} V_s &= \frac{1}{2}\int_{-1}^{1} d\cos\theta \frac{1}{-|\vec{k}|^2 - |\vec{k}'|^2 + 2|\vec{k}||\vec{k}'|\cos\theta - m_\rho^2} \\ &= \frac{1}{4|\vec{k}|^2}\ln\frac{m_\rho^2}{m_\rho^2 + 4|\vec{k}|^2} \end{aligned} \tag{18}$$

with $|\vec{k}'|^2 = |\vec{k}|^2$ given by eq. (15). When we neglect q^2 this potential is $(-m_\rho^2)^{-1}$ such that the ratio of the on-shell s-wave projected potential to the static one is given by

$$R = \frac{m_\rho^2}{4|\vec{k}|^2}\ln\frac{m_\rho^2 + 4|\vec{k}|^2}{m_\rho^2} \tag{19}$$

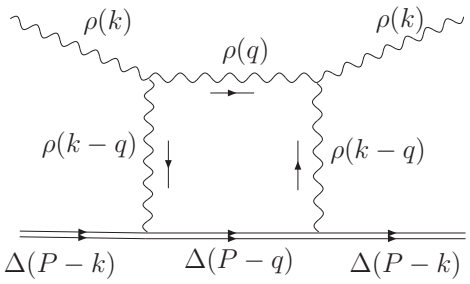

Figure 5: Term with intermediate $\rho\Delta$ in the $\rho\Delta \to \rho\Delta$ interaction, involving the $\rho\rho\rho$ coupling.

eq. (18) shows the singularity which appears when eq. (16) is fulfilled. Once we reach this point it is interesting to visualize the meaning and extent of the on-shell factorization of the N/D method. Let us now evaluate the Feynman box diagram of fig. 5. We take all vertices equal to unity since we simply want to compare with the on-shell factorization. We evaluate the loop function given by

$$\begin{aligned} L &= 2iM_\Delta \int \frac{d^4q}{(2\pi)^4} \frac{1}{q^2 - m_\rho^2 + i\epsilon} \left(\frac{1}{(k-q)^2 - m_\rho^2 + i\epsilon} \right)^2 \frac{1}{(P-q)^2 - M_\Delta^2 + i\epsilon} \\ &= 2iM_\Delta \frac{\partial}{\partial m_\rho^2} \int \frac{d^4q}{(2\pi)^4} \frac{1}{q^2 - m_\rho'^2 + i\epsilon} \frac{1}{(k-q)^2 - m_\rho^2 + i\epsilon} \frac{1}{(P-q)^2 - M_\Delta^2 + i\epsilon} \end{aligned} \quad (20)$$

where m'_ρ will be made equal to m_ρ after the derivative. Using standard Feynman integral techniques we can write L as

$$L = -\frac{1}{16\pi^2} 2M_\Delta \int_0^1 dx(1-x) \int_0^x \frac{dy}{(s' + i\epsilon)^2} \quad (21)$$

where

$$s' = (x - 1 - x^2)m_\rho^2 - sy^2 + xy(s + m_\rho^2 - M_\Delta^2) \quad (22)$$

In the on-shell factorization this integral would correspond to

$$L \to V_s^2 \; G \quad (23)$$

where G is the $\rho\Delta$ loop function of eq. (10). In fig. 6 we compare L/V_s^2 obtained from eqs. (18) and (21) with G as a function of the energy. The idea behind the on-shell factorization is that the two sides of eq. (23) are equivalent with a suitable subtraction constant in the function G, which requires regularization since it is logarithmically divergent. The subtraction constant in G has been chosen such that the two functions are equal at the $\rho\Delta$ threshold, the cusp point. As we can see, the on-shell factorization and the Feynman integral are remarkably similar in the region of interest to us in this sector, 1850 MeV - 2000 MeV [32], down to values of s very close to the branch point of the t-channel. The

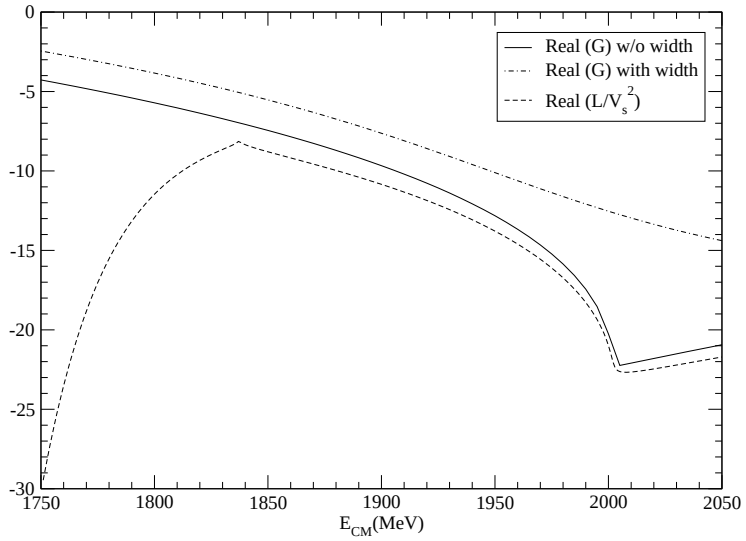

Figure 6: (L/V_s^2) as a function of the energy. The G function after convolution with the spectral function of the ρ and the Δ to account for their width is also shown for comparison.

differences are small compared to the effects of taking into account the ρ and the Δ mass distributions. We will come back to this point again when mentioning coupled channels, where we shall recall the main point of the former discussion, which is the absolute failure of this on shell factorization below the branch point.

Let us now turn our attention to the left hand cut related to the u-channel. For this purpose let us look at fig. 7. The intermediate Δ propagator reads

$$G_\Delta = \frac{1}{\sqrt{s} - \omega_\rho(k) - \omega_\rho(k') - E_\Delta(\vec{k} + \vec{k}')} \tag{24}$$

Taking again the usual on-shell prescription of $p^2 = m^2$ for the external legs we find the pole of eq. (24) at highest energy when $\vec{k}$ and $\vec{k}'$ are equal. Substituting the on-shell values of k of eq. (15) we find the solution

$$s = M_\Delta^2 + 2m_\rho^2 \tag{25}$$

which sets the branch point of the u-channel at $\sqrt{s} = 1644$ MeV. This is far away from the region of interest so that we can safely neglect it. However, when considering coupled channels the branch point moves to higher energies in other channels. We will come back to this issue a little later. Should we have just this channel there is no cause for concern since we can incorporate s-wave contributions from this channel with a suitable subtraction constant in the G function. There is more to it since we can make explicit evaluations of the s-wave contribution of the u-channel. For this we project the propagator of eq. (24) over s-wave, as done in eq. (18), taking the $\gamma^0\epsilon^0$ component, approximated by k/M_V for

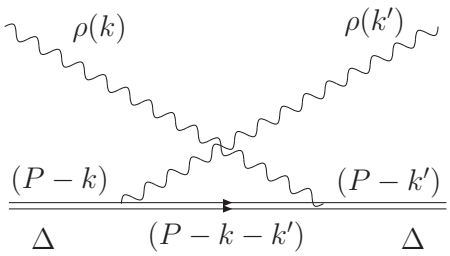

Figure 7: $\Delta\rho$ scattering diagram in the u-channel.

the $\rho\Delta$ coupling (the spatial components lead to p-waves mostly) and we find

$$V_s(k) = \frac{M_\Delta}{2m_\rho^2} g^2 \ln \frac{\sqrt{s} - 2\omega_\rho(k) - M_\Delta}{\sqrt{s} - 2\omega_\rho(k) - (M_\Delta^2 + 4|\vec{k}|^2)^{1/2}} \tag{26}$$

If we compare this with the dominant t-channel ρ exchange projected over s-wave, which is of the order of $2g^2\omega_\rho(k)/(-m_\rho^2)$ multiplied by R of eq. (19), we see that the ratio is of the order of 5 % for $\sqrt{s}$ above 1850 MeV and thus negligible. This is without counting extra C factors of eq. (9) , which tend to make the ratio even smaller. For all these reasons the u-channel can be safely neglected when dealing with the s-wave interaction.

We now come back to the t-channel branch points for the coupled channels. In the case of the $\rho\Delta$ interaction we have also the coupled channel $K^*\Sigma^*$. In the diagonal transition $K^*\Sigma^* \to K^*\Sigma^*$ we have also the ρ as the lightest vector exchanged. Substituting $\rho\Delta$ by $K^*\Sigma^*$ in eq. (15) together with eq. (16) lead now to the branch point at $\sqrt{s} = 2133$ MeV. This energy is bigger than the energy of the two states that we obtain around 1850 MeV and 1950 MeV [32] and calls for some reflection. As we could see from the discussion that lead to fig. 6, the region of energies of interest to us around 1800 MeV-2000 MeV is about 250 MeV below the branching point of the $K^*\Sigma^*$ channel and the on shell factorization of the ρ exchange in the $K^*\Sigma^* \to K^*\Sigma^*$ potential would simply be ruled out. This apparent failure is something which is welcome, because one can trace it to an abuse of the standard procedure used in one channel problems, which needs to be changed for coupled channels. Indeed, the blind application of the on-shell factorization would imply using momenta of the K^* of the order of $i300$ MeV; purely imaginary. Obviously this is meaningless from the physical point of view. The states that we have are a mixture of $\rho\Delta$ and $K^*\Sigma^*$ and have a certain energy, around 1850 MeV and 1950 MeV [32], as we shall see. However, the momentum of these components has to be a real quantity, which implies that the $K^*\Sigma^*$ are very bound. This is the physical world for bound states. The "on-shell" result that the K^* has an imaginary momentum stems from the fact that we impose $p^2 = m^2$ for the K^* and the Σ^*, which is definitely not the case in the real situation. However, in one channel problems, the extrapolation to the complex plane imposing $p^2 = m^2$ is a customary procedure. It is very useful because with the extrapolation to the complex plane one can make use of complex variable theorems and come out with valuable results

from dispersion relations. Yet, one should not forget that the extrapolated amplitudes to the unphysical regions have no physical meaning, and particularly the imaginary momenta cannot be confused with the actual momenta of the particles.

We thus see that in the case of coupled channels, one must invoke the binding of the components, but the momenta will always be real. The size of the momenta will be typical of the momentum distribution of bound states of hadrons with masses similar to those of the vector mesons. Nuclei are something of this sort, with nucleons bound by about 60 MeV, and momenta of the order of 200 MeV as average. If we take this range, $(\vec{q}/M_V)^2$ is of the order of 5 % and a realistic "on-shell" factorization of the ρ propagator for the physical states would give essentially $-1/m_\rho^2$. Obviously now $p^2 \neq m^2$ for the external lines. The K^*, Σ^* are now very bound, much like the Δ components are bound in ordinary nuclei [36, 37].

There are more arguments to support the use of that approximation in the vector meson propagators. Indeed, we are dealing with a coupled set of Bethe Salpeter equations. One way to deal with the Bethe Salpeter equation is to solve the integral equation, in which case a form factor is usually put to make the integrals converge [34, 35]. The cut off is fitted to some data, usually the mass of some state, or a scattering length. We note that in these and other works, the vector propagator is kept together with one additional form factor, usually a static form factor [35]. Together they impose a range to the interaction. We would like to state here that if the form factor is going to be fitted to experiment, one can as well neglect the $\vec{q}$ dependence of the propagator and fit a global form factor to the data. Keeping this in mind, we resort to the easy, and equivalent procedure of not putting any form factor but cutting the loop integrals at a maximum value of the three-momentum. In other words, we would be introducing a global static form factor which is a theta function. The parameter to fit in this case if the cut off momentum, or taking into account the equivalence of this procedure with dimensional regularization [9], fixing the subtraction constant. We make use of this latter procedure. The approach has technical advantages; the potential now factorizes in the loops and then only the integrals of two propagators need to be performed and the set of Bethe Salpeter equations becomes now a set of algebraic equations. The procedure is equivalent to using the on-shell factorization, but with a potential with no $\vec{q}$ dependence which corresponds to a constant, *i.e.* a local term with no left hand cut. This is the way our equations must be visualized and the precise meaning of the on-shell factorization, often employed when dealing with these equations.

The arguments used here for the t-channel can be extended to the u-channel in the case of coupled channels, where one would bind the external particles and have real momenta. The corrections of these terms are then very small, as we saw, and of the type $(\vec{k}/M_V)^2$.

There is another issue that must be raised at this point. As described in detail in [35] one has some flexibility to describe the same results changing simultaneously the form factor and the strength of the interaction. We also observe the same pattern by changing simultaneously the potential and the cut off, or subtraction constant. This is important to keep in mind in order to correct for approximations made in the potential. In this sense, our procedure is as follows. We obtain the strength of the potential from the theoretical approach, then take a cut off around 1 GeV, typical of the effective theories in the range of

energies that we are considering and see that we obtain a bound state or resonance close to some physical state, to which the identification is likely. After that, there is a small tuning of the cut off or subtraction constant such as to get the position of this state at a precise experimental energy. Later on the same cut off, subtraction constant in our case, is used to determine all the amplitudes and bound states or resonances in other channels. Let us assume we had just one bound state not far from threshold (the argument also holds qualitatively for many channels when one of them clearly dominates). Let us then keep in mind that our description of the states comes through the couplings of the resonances to the different channels. In the case of just one channel the coupling is given in terms of the binding energy according to the Weinberg compositness condition [38, 39, 40, 41]. The theorem can be restated in the formalism used here, as shown in [42], where one can see that the coupling depends exclusively on the derivative of the G function at the pole position independently of the potential. Our fitting procedure to the mass of one state undoubtedly benefits from this theorem that guaranties a good coupling in the case of one channel, or dominance of one channel in the coupled channel case. The procedure of fixing one state also provides a better stability of the theoretical results for the nearby states since the difference of masses can always be better predicted than absolute ones.

One more comment concerning the work of [35] is in order. The results "beyond the zero range approximation" reported there take into account the range of the exchanged vector mesons and an extra static form factor is used. The main effect observed there is an increase of the non diagonal potentials mostly because of the energy transfer in the vector propagators. This has as a result a moderate increase of the widths of the states. The positions are practically unchanged. This energy transfer is sometimes non negligible in [35] because the authors are dealing with charmed mesons and baryons where the differences of masses with respect to non charmed hadrons are large. The same corrections are taken into account in [43]. In the present case we deal with vector mesons in SU(3) which have very similar masses and that feature does not appear.

After this discussion, justifying the approach presented at the beginning of section 2, we move on to show the results obtained.

3 Results

In this section we show results for the amplitudes obtained in the attractive channels mentioned above. In figs. 8, 9 and 10 we show the results for the channels $S, I = 0, 1/2$; $0, 3/2$; $-1, 0$; $-1, 1$; $-2, 1/2$ and $-3, 0$. The value of $a_l(\mu)$ taken is -2.2 MeV.

3.1 S,I=0,1/2 states

The figures show peaks of $|T|^2$ which indicate the existence of a pole or a resonance. To further verify the guess, we look for poles in the complex plane as done in [8, 9, 23]. The real part of the pole position provides the mass of the resonance and two times the imaginary part its width. The results can be seen in tables 11, 12, 13, 14, 15, 16. In

fig. 8 we show the results for the $S, I = 0, 1/2;\ 0, 3/2$ channels. In the $S, I = 0, 1/2$ sector (fig. 8(left)) we see a clear peak around 1850 MeV, most pronounced in the $\Delta\rho$ channel, but also visible in $\Sigma^* K^*$. This is also reflected in the couplings in table 11. This difference in the couplings and the large mass difference of the $\Sigma^* K^*$ state with respect to the mass of the resonance makes the effect of this channel essentially negligible and the state qualifies cleanly as a $\Delta\rho$ state, as was assumed in [32]. The second weak structure around 2270 MeV on the $\Sigma^* K^*$ threshold does not correspond to a pole. Note, however, that such a bump could be identified experimentally with a resonance. In fact, there is a cataloged resonance $N^*(2200)(5/2^-)$ around that energy.

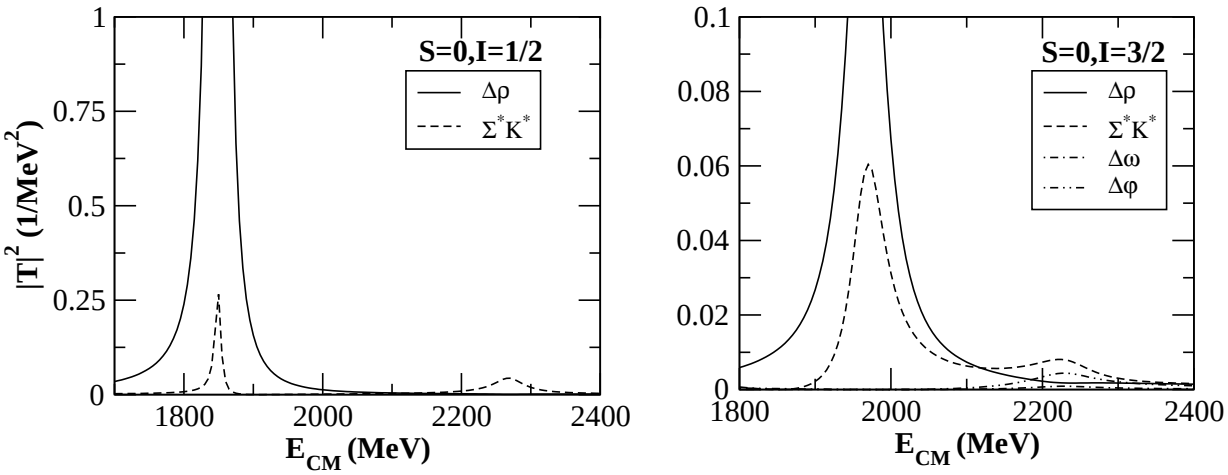

Figure 8: $|T|^2$ for $S, I = 0, 1/2$ and $0, 3/2$.

3.2 S,I=0,3/2 states

In this case we see a clear peak in fig. 8(right) that shows mostly in the $\Delta\rho$ channel. An inspection of table 12 also indicates substantial coupling to the $\Sigma^* K^*$ channel. This state was obtained in [32] considering only the $\Delta\rho$ channel. A posteriori, we corroborate the approach of [32] which was justified there in the fact that the lowest mass states should be constructed with the lowest mass vector and meson. The channel $\Delta\omega$ which has about the same mass as that of the $\Delta\rho$ was ignored in [32] since, as one can see in table 3, it does not couple to the $\Delta\rho$ nor to itself. Now the final coupling of the $\Delta\omega$ to the resonance is not zero, although negligible. The reason is that the coupled channel treatment allows this resonance to couple to $\Delta\omega$ through non diagonal transitions to the $\Sigma^* K^*$ state. The weaker broad structure that appears around 2200 MeV in the $\Sigma^* K^*$ channel does not correspond to a pole in the complex plane. However, we should note that with a slightly weaker subtraction constant, $a = -2.1$, it shows much more neatly and around 2150 MeV, and could be associated with the cataloged $\Delta(2150)(1/2^-)$.

3.3 S,I=-1,0 states

In fig. 9(left) we find a clear peak around 2050 MeV which is most visible in the $\Sigma^*\rho$ channel but also couples to the Ξ^*K^*. This is corroborated by the strength of the couplings in table 13. There is a weaker structure in the Ξ^*K^* channel around 2400 MeV (at threshold) which does not correspond to a pole in the complex plane.

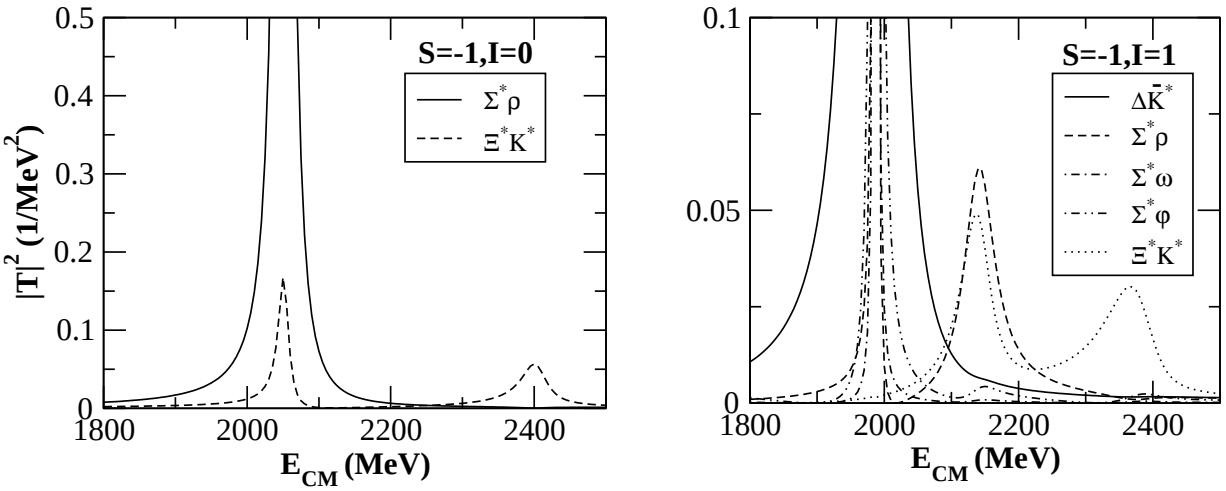

Figure 9: $|T|^2$ for $S, I = -1, 0$ and $-1, 1$.

3.4 S,I=-1,1 states

Fig 9(right) shows this case where there are five coupled channels producing three structures in the amplitude squared which indeed correspond to three poles as shown in table 14. The first around 1990 MeV couples strongly to $\Delta\bar{K}^*$, another one near 2150 MeV that couples strongly to $\Sigma^*\rho$ and Ξ^*K^*, and a third broader one around 2380 MeV that couples mostly to Ξ^*K^*.

3.5 S,I=-2,1/2 states

In this case also there are five coupled channels. One finds three clear structures in fig 10(left) which correspond to three poles of the scattering amplitude. The one around 2200 MeV couples mostly to $\Sigma^*\bar{K}^*$ and $\Xi^*\phi$ as seen from table 15. The second, around 2300 MeV is seen prominently in the $\Xi^*\rho$ channel. The other around 2520 MeV couples mostly to ΩK^* and appears as a distinct peak structure in this channel.

3.6 S,I=-3,0 states

We see in fig. 10(right) a clear peak around 2450 MeV corresponding to a pole in the complex energy plane around this energy. As seen from table 16, this state couples mostly to $\Omega\phi$ and $\Omega\omega$.

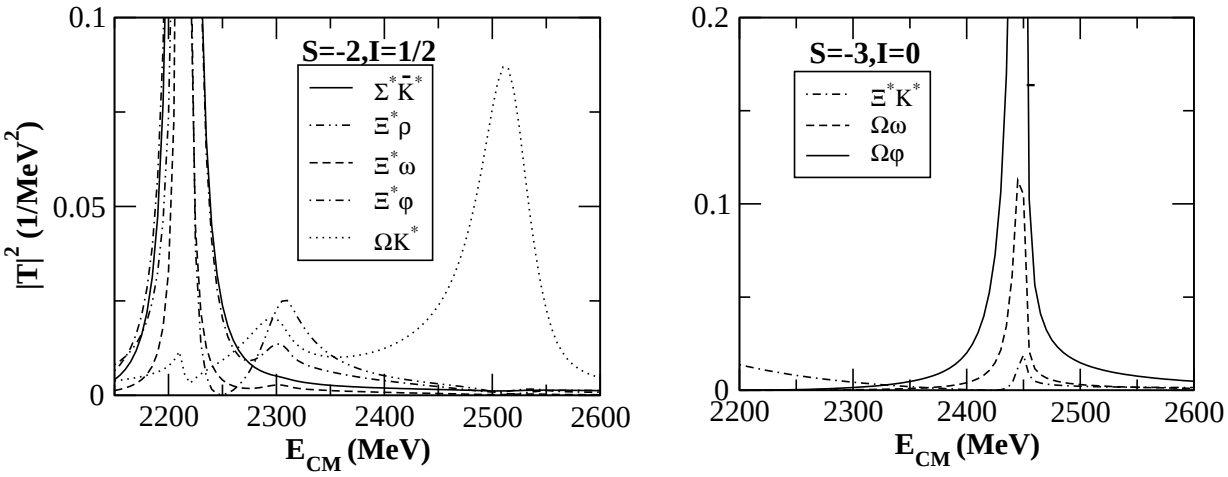

Figure 10: $|T|^2$ for $S, I = -2, 1/2$ and $-3, 0$.

4 Comparison to data

It is interesting to compare with data of the PDG. A summary is presented in table 1 in which the 10 dynamically generated states have been listed along with their possible PDG counterparts including their present status and properties. The two states that we find for $S, I = 0, 1/2$ and $0, 3/2$ around 1850 MeV and 1970 MeV respectively were discussed in detail in [32]. We do not discuss them further but recall that there are indeed natural candidates for these states in the $\Delta(1900)$ $3/2(1/2^-)$, $\Delta(1940)$ $3/2(3/2^-)\Delta(1930)$ $3/2(5/2^-)$. As discussed there, some fine tuning of the subtraction constant can make the masses agree better. But differences of 50 MeV or more are the state of the art in determining masses in hadronic models. As to the N^* states around these energies, we mention, recalling [32] that there is a large dispersion of data in the masses but there are indeed several candidate states like the $N^*(2090)$ $1/2(1/2^-)$, $N^*(2080)$ $1/2(3/2^-)$ etc. though some of the states predicted could be missing.

The Λ^* state that we see in $S, I = -1, 0$ around 2050 MeV could correspond to the $\Lambda(2000)$ with spin parity unknown. We do not see traces of the spin partners in this energy region.

In the Σ^* sector we found three states around 1990, 2150, 2380 MeV. One can find two states around 2000 MeV in table 1, $\Sigma(1940)$ $(3/2^-)$ and $\Sigma(2000)$ $(1/2^-)$. At higher energies there are several states. One of them, the $\Sigma^*(2250)$ classified with three stars, where some experiments see two resonances, one of them with $5/2^-$. Another one is the $\Sigma^*(2455)$ classified as bumps without spin and parity assignment. This region is the experimental frontier in this sector and we hope that the findings of the present work stimulate further work to complete the table. Indeed, the information we provide, telling to which states the resonance couples most strongly could be a guiding line for the search of these new states.

In the Ξ^*, $S, I = -2, 1/2$ sector we find three states around 2200 MeV, 2300 MeV and 2520 MeV. As shown in table 1 in the PDG, we find three states $\Xi(2250)$, $\Xi(2370)$, $\Xi(2500)$

S, I	Theory			PDG data				
	pole position	real axis		name	J^P	status	mass	width
		mass	width					
$0, 1/2$	$1850 + i5$	1850	11	$N(2090)$	$1/2^-$	$\star$	1880-2180	95-414
				$N(2080)$	$3/2^-$	$\star\star$	1804-2081	180-450
		2270(*bump*)		$N(2200)$	$5/2^-$	$\star\star$	1900-2228	130-400
$0, 3/2$	$1972 + i49$	1971	52	$\Delta(1900)$	$1/2^-$	$\star\star$	1850-1950	140-240
				$\Delta(1940)$	$3/2^-$	$\star$	1940-2057	198-460
				$\Delta(1930)$	$5/2^-$	$\star\star\star$	1900-2020	220-500
		2200(*bump*)		$\Delta(2150)$	$1/2^-$	$\star$	2050-2200	120-200
$-1, 0$	$2052 + i10$	2050	19	$\Lambda(2000)$	$?^?$	$\star$	1935-2030	73-180
$-1, 1$	$1987 + i1$	1985	10	$\Sigma(1940)$	$3/2^-$	$\star\star\star$	1900-1950	150-300
	$2145 + i58$	2144	57	$\Sigma(2000)$	$1/2^-$	$\star$	1944-2004	116-413
	$2383 + i73$	2370	99	$\Sigma(2250)$	$?^?$	$\star\star\star$	2210-2280	60-150
				$\Sigma(2455)$	$?^?$	$\star\star$	2455±10	100-140
$-2, 1/2$	$2214 + i4$	2215	9	$\Xi(2250)$	$?^?$	$\star\star$	2189-2295	30-130
	$2305 + i66$	2308	66	$\Xi(2370)$	$?^?$	$\star\star$	2356-2392	75-80
	$2522 + i38$	2512	60	$\Xi(2500)$	$?^?$	$\star$	2430-2505	59-150
$-3, 0$	$2449 + i7$	2445	13	$\Omega(2470)$	$?^?$	$\star\star$	2474±12	72±33

Table 1: The properties of the 10 dynamically generated resonances and their possible PDG counterparts. We also include the N^* bump around 2270 MeV and the Δ^* bump around 2200 MeV.

with spin and parity unknown. This sector is also poorly known but an experimental program is running at Jefferson Lab to widen the information in this sector [48, 49].

Finally, in the Ω sector we find a clean state around 2450 MeV. Once again we find in the PDG the $\Omega(2470)$ without spin and parity assigned.

The width of the resonances in the present framework is given by twice the imaginary part of the pole position in the complex energy plane. Also reported in the 'real-axis' column of table 1 is the full width at half maximum obtained from the square of the amplitude plotted as a function of energy. However, we do not consider it meaningful

to compare the widths of the dynamically generated states with those of the PDG in this work. Those reported here correspond only to decay into the vector-baryon decuplet states. In addition there are decays into a pseudoscalar meson and an octet baryon which can also be calculated in this approach, in a similar way as it was done in [25] to obtain the decay into $\pi\pi$ of the $\rho\rho$ states found there. Given the incomplete information about the states in the PDG in this area and the qualitative assignments that we can only do at present, its evaluation would not provide more help establishing the association of theoretical states with the experimental ones, but when the situation improves, this work could be done to help understand better the spectrum of baryons.

5 Conclusions

We have studied the interaction of vector mesons with the decuplet of baryons, looking for bound states or resonances, and we find ten poles in the scattering matrices of different strangeness and isospin channels. The states are furthermore degenerate in $J^P = 1/2^-, 3/2^-, 5/2^-$. We found candidates in the PDG to be associated to the states found, but many of them are missing. This should not be a surprise since the states we find are at the frontier of the experimental research. The success of the method applied in other sectors, as the meson sector, and even here for the lowest energy states found, makes us confident that these states exist. The difficulties in finding them are understandable. Most of the states reported in this energy region are found in partial wave analysis of reactions using the available pion, photon, electron or kaon beams. Some of these analyses require the simultaneous consideration of many resonances, more than twenty in some cases, which makes the conclusions problematic. Indeed, different solutions are often found, concerning not only the properties but even the existence of some resonances, depending on the type of analysis or the assumptions made. New schemes become necessary to make progress in this area. In this sense, the present theoretical work, as well as others, where predictions are made regarding the channels to which the resonances couple most strongly, could be considered as a guideline to search for specific final states which could filter some of the resonances. We envisage a fruitful new strategy of research along this line and encourage future work in this direction.

Acknowledgments

B. X. Sun would like to thank Li-Sheng Geng and R. Molina for useful discussions. This work is partly supported by DGICYT contract number FIS2006-03438. This research is part of the EU Integrated Infrastructure Initiative Hadron Physics Project under contract number RII3-CT-2004-506078. B. X. Sun acknowledges support from the National Natural Science Foundation of China under grant number 10775012.

References

[1] J. A. Oller and E. Oset, Nucl. Phys. A **620**, 438 (1997) [Erratum-ibid. A **652**, 407 (1999)] [arXiv:hep-ph/9702314].

[2] J. A. Oller, E. Oset and J. R. Pelaez, Phys. Rev. D **59**, 074001 (1999) [Erratum-ibid. D **60**, 099906 (1999 ERRAT,D75,099903.2007)] [arXiv:hep-ph/9804209].

[3] N. Kaiser, Eur. Phys. J. A **3**, 307 (1998).

[4] V. E. Markushin, Eur. Phys. J. A **8**, 389 (2000) [arXiv:hep-ph/0005164].

[5] N. Kaiser, P. B. Siegel and W. Weise, Phys. Lett. B **362**, 23 (1995) [arXiv:nucl-th/9507036].

[6] N. Kaiser, P. B. Siegel and W. Weise, Nucl. Phys. A **594**, 325 (1995) [arXiv:nucl-th/9505043].

[7] N. Kaiser, T. Waas and W. Weise, Nucl. Phys. A **612**, 297 (1997) [arXiv:hep-ph/9607459].

[8] E. Oset and A. Ramos, Nucl. Phys. A **635** (1998) 99 .

[9] J. A. Oller and U. G. Meissner, Phys. Lett. B **500**, 263 (2001) [arXiv:hep-ph/0011146].

[10] C. Garcia-Recio, M. F. M. Lutz and J. Nieves, Phys. Lett. B **582** (2004) 49 .

[11] C. Garcia-Recio, J. Nieves and L. L. Salcedo, Phys. Rev. D **74** (2006) 034025 .

[12] T. Hyodo, S. I. Nam, D. Jido and A. Hosaka, Phys. Rev. C **68**, 018201 (2003) [arXiv:nucl-th/0212026].

[13] T. Hyodo, D. Jido and A. Hosaka, Phys. Rev. D **75**, 034002 (2007) [arXiv:hep-ph/0611004].

[14] T. Inoue, E. Oset and M. J. Vicente Vacas, Phys. Rev. C **65**, 035204 (2002) [arXiv:hep-ph/0110333].

[15] E. E. Kolomeitsev and M. F. M. Lutz, Phys. Lett. B **585** (2004) 243 .

[16] S. Sarkar, E. Oset and M. J. Vicente Vacas, Nucl. Phys. A **750** (2005) 294 [Erratum-ibid. A **780** (2006) 78] .

[17] D. Jido, J. A. Oller, E. Oset, A. Ramos and U. G. Meissner, Nucl. Phys. A **725**, 181 (2003) [arXiv:nucl-th/0303062].

[18] S. Prakhov *et al.* [Crystall Ball Collaboration], Phys. Rev. C **70**, 034605 (2004).

[19] V. K. Magas, E. Oset and A. Ramos, Phys. Rev. Lett. **95**, 052301 (2005) [arXiv:hep-ph/0503043].

[20] I. Zychor *et al.*, Phys. Lett. B **660**, 167 (2008) [arXiv:0705.1039 [nucl-ex]].

[21] L. S. Geng, E. Oset and M. Doring, Eur. Phys. J. A **32**, 201 (2007) [arXiv:hep-ph/0702093].

[22] M. F. M. Lutz and E. E. Kolomeitsev, Nucl. Phys. A **730**, 392 (2004) [arXiv:nucl-th/0307039].

[23] L. Roca, E. Oset and J. Singh, Phys. Rev. D **72**, 014002 (2005) [arXiv:hep-ph/0503273].

[24] L. S. Geng, E. Oset, L. Roca and J. A. Oller, Phys. Rev. D **75**, 014017 (2007) [arXiv:hep-ph/0610217].

[25] R. Molina, D. Nicmorus and E. Oset, Phys. Rev. D **78**, 114018 (2008) [arXiv:0809.2233 [hep-ph]].

[26] M. Bando, T. Kugo, S. Uehara, K. Yamawaki and T. Yanagida, Phys. Rev. Lett. **54**, 1215 (1985).

[27] M. Bando, T. Kugo and K. Yamawaki, Phys. Rept. **164**, 217 (1988).

[28] M. Harada and K. Yamawaki, Phys. Rept. **381**, 1 (2003) [arXiv:hep-ph/0302103].

[29] H. Nagahiro, J. Yamagata-Sekihara, E. Oset and S. Hirenzaki, arXiv:0809.3717 [hep-ph].

[30] L. S. Geng and E. Oset, Phys. Rev. D **79**, 074009 (2009) arXiv:0812.1199 [hep-ph].

[31] C. Amsler *et al.* [Particle Data Group], Phys. Lett. B **667**, 1 (2008).

[32] P. Gonzalez, E. Oset and J. Vijande, Phys. Rev. C **79**, 025209 (2009) [arXiv:0812.3368 [hep-ph]].

[33] J. A. Oller and E. Oset, Phys. Rev. D **60**, 074023 (1999) [arXiv:hep-ph/9809337].

[34] A. D. Lahiff and I. R. Afnan, Phys. Rev. C **60**, 024608 (1999) [arXiv:nucl-th/9903058].

[35] C. E. Jimenez-Tejero, A. Ramos and I. Vidana, arXiv:0907.5316 [hep-ph].

[36] H. J. Weber and H. Arenhovel, Phys. Rept. **36** (1978) 277.

[37] M. A. Moinester and H. J. Lipkin, Phys. Lett. B **277**, 221 (1992).

[38] S. Weinberg, Phys. Rev. **130**, 776 (1963).

[39] G. V. Efimov and M. A. Ivanov, IOP Publishing, Bristol & Philadelphia (1993).

[40] V. Baru, J. Haidenbauer, C. Hanhart, Yu. Kalashnikova and A. E. Kudryavtsev, Phys. Lett. B **586**, 53 (2004) [arXiv:hep-ph/0308129].

[41] Y. b. Dong, A. Faessler, T. Gutsche and V. E. Lyubovitskij, Phys. Rev. D **77**, 094013 (2008) [arXiv:0802.3610 [hep-ph]].

[42] D. Gamermann and E. Oset, Phys. Rev. D 80 (2009) 014003, arXiv:0905.0402 [hep-ph].

[43] A. Martinez Torres, K. P. Khemchandani, D. Gamermann and E. Oset, arXiv:0906.5333 [nucl-th].

[44] D. Cabrera, E. Oset and M. J. Vicente Vacas, Nucl. Phys. A **705**, 90 (2002) [arXiv:nucl-th/0011037].

[45] H. Nagahiro, L. Roca, A. Hosaka and E. Oset, Phys. Rev. D **79**, 014015 (2009) [arXiv:0809.0943 [hep-ph]].

[46] E. Oset, D. Cabrera, V.K. Magas, L. Roca, S.Sarkar, M.J. Vicente Vacas and A. Ramos, Pramana**66**, 731 (2006) [arXiv:nucl-th/0504033].

[47] M. Kirchbach and C. B. Compean, Eur. Phys. J. A 39, 1 (2007) arXiv:0805.2404 [hep-ph].

[48] B. M. K. Nefkens, AIP Conf. Proc. **870**, 405 (2006).

[49] J. W. Price *et al.* [CLAS Collaboration], Phys. Rev. C **71**, 058201 (2005) [arXiv:nucl-ex/0409030].

6 Appendix

	$\Delta\rho$	$\Sigma^* K^*$
$\Delta\rho$	5	2
$\Sigma^* K^*$		2

Table 2: C_{ij} coefficients for $S = 0$, $I = \frac{1}{2}$.

	$\Delta\rho$	$\Sigma^* K^*$	$\Delta\omega$	$\Delta\phi$
$\Delta\rho$	2	$\sqrt{\frac{5}{2}}$	0	0
$\Sigma^* K^*$		-1	$\sqrt{\frac{3}{2}}$	$-\sqrt{3}$
$\Delta\omega$			0	0
$\Delta\phi$				0

Table 3: C_{ij} coefficients for $S = 0$, $I = \frac{3}{2}$.

	$\Sigma^* \rho$	$\Xi^* K^*$
$\Sigma^* \rho$	4	$\sqrt{6}$
$\Xi^* K^*$		3

Table 4: C_{ij} coefficients for $S = -1$, $I = 0$.

	$\Delta\overline{K}^*$	$\Sigma^*\rho$	$\Sigma^*\omega$	$\Sigma^*\phi$	Ξ^*K^*
$\Delta\overline{K}^*$	4	1	$\sqrt{2}$	-2	0
$\Sigma^*\rho$		2	0	0	2
$\Sigma^*\omega$			0	0	$\sqrt{2}$
$\Sigma^*\phi$				0	-2
Ξ^*K^*					1

Table 5: C_{ij} coefficients for $S = -1$, $I = 1$.

	$\Delta\overline{K}^*$	$\Sigma^*\rho$
$\Delta\overline{K}^*$	0	$\sqrt{3}$
$\Sigma^*\rho$		-2

Table 6: C_{ij} coefficients for $S = -1$, $I = 2$.

	$\Sigma^*\overline{K}^*$	$\Xi^*\rho$	$\Xi^*\omega$	$\Xi^*\phi$	ΩK^*
$\Sigma^*\overline{K}^*$	2	1	$\sqrt{3}$	$-\sqrt{6}$	0
$\Xi^*\rho$		2	0	0	$\frac{3}{\sqrt{2}}$
$\Xi^*\omega$			0	0	$\sqrt{\frac{3}{2}vd_rev - 0416 - ch}$
$\Xi^*\phi$				0	$-\sqrt{3}$
ΩK^*					3

Table 7: C_{ij} coefficients for $S = -2$, $I = \frac{1}{2}$.

	$\Sigma^*\overline{K}^*$	$\Xi^*\rho$
$\Sigma^*\overline{K}^*$	-1	2
$\Xi^*\rho$		-1

Table 8: C_{ij} coefficients for $S = -2$, $I = \frac{3}{2}$.

	$\Xi^*\overline{K}^*$	$\Omega\omega$	$\Omega\phi$
$\Xi^*\overline{K}^*$	0	$\sqrt{3}$	$-\sqrt{6}$
$\Omega\omega$		0	0
$\Omega\phi$			0

Table 9: C_{ij} coefficients for $S = -3$, $I = 0$.

	$\Xi^*\overline{K}^*$	$\Omega\rho$
$\Xi^*\overline{K}^*$	-2	$\sqrt{3}$
$\Omega\rho$		-2

Table 10: C_{ij} coefficients for $S = -3$, $I = 1$.

z_R	$1850 + i5$	
	g_i	$\lvert g_i\rvert$
$\Delta\rho$	$4.9 + i0.1$	4.9
Σ^*K^*	$1.7 + i0.0$	1.7

Table 11: The position of the pole and the coupling constant g_i of the resonance for $S = 0$, $I = \frac{1}{2}$.

z_R	$1972 + i49$	
	g_i	$\lvert g_i\rvert$
$\Delta\rho$	$5.0 + i0.2$	5.0
Σ^*K^*	$3.9 - i0.1$	3.9
$\Delta\omega$	$-0.1 + i0.2$	0.3
$\Delta\phi$	$0.2 - i0.4$	0.4

Table 12: The position of the pole and the coupling constant g_i of the resonance for $S = 0$, $I = \frac{3}{2}$.

z_R	$2052 + i10$	
	g_i	$\|g_i\|$
$\Sigma^*\rho$	$4.2 + i0.1$	4.2
Ξ^*K^*	$2.0 + i0.1$	2.0

Table 13: The position of the pole and the coupling constant g_i of the resonance for $S = -1$, $I = 0$.

z_R	$1987 + i1$		$2145 + i58$		$2383 + i73$	
	g_i	$\|g_i\|$	g_i	$\|g_i\|$	g_i	$\|g_i\|$
$\Delta\overline{K^*}$	$4.2 + i0.0$	4.2	$0.7 + i0.1$	0.7	$0.4 + i0.4$	0.6
$\Sigma^*\rho$	$1.4 + i0.0$	1.4	$-4.3 - i0.7$	4.4	$0.4 + i1.1$	1.2
$\Sigma^*\omega$	$1.4 + i0.0$	1.4	$1.3 - i0.4$	1.3	$-1.4 - i0.4$	1.5
$\Sigma^*\phi$	$-2.1 - i0.0$	2.1	$-1.9 + i0.6$	2.0	$2.1 + i0.6$	2.2
Ξ^*K^*	$0.1 - i0.0$	0.1	$-4.0 - i0.1$	4.0	$-3.5 + i1.5$	3.8

Table 14: The position of the pole and the coupling constant g_i of the resonance for $S = -1$, $I = 1$.

z_R	$2214 + i4$		$2305 + i66$		$2522 + i38$	
	g_i	$\|g_i\|$	g_i	$\|g_i\|$	g_i	$\|g_i\|$
$\Sigma^*\overline{K^*}$	$2.4 + i0.1$	2.4	$0.8 - i0.1$	0.8	$0.3 + i0.3$	0.4
$\Xi^*\rho$	$1.8 - i0.1$	1.8	$-3.5 - i1.7$	3.9	$0.2 + i1.0$	1.0
$\Xi^*\omega$	$1.7 + i0.1$	1.7	$2.0 - i0.7$	2.1	$-0.6 - i0.3$	0.7
$\Xi^*\phi$	$-2.5 - i0.1$	2.5	$-3.0 + i1.0$	3.1	$0.9 + i0.4$	1.0
ΩK^*	$0.5 - i0.1$	0.5	$-2.7 - i0.8$	2.8	$-3.3 + i0.9$	3.4

Table 15: The position of the pole and the coupling constant g_i of the resonance for $S = -2$, $I = 1/2$.

z_R	$2449 + i7$	
	g_i	$\|g_i\|$
$\Xi^*\overline{K^*}$	$1.0 + i0.2$	1.0
$\Omega\omega$	$1.6 - i0.2$	1.7
$\Omega\phi$	$-2.4 + i0.3$	2.5

Table 16: The position of the pole and the coupling constant g_i of the resonance for $S = -3$, $I = 0$.